Nanoscale

PAPER

View Article Online
View Journal | View Issue



Cite this: *Nanoscale*, 2014, **6**, 11795

# Vertically stacked plasmonic nanoparticles in a circular arrangement: a key to colorimetric refractive index sensing†

Sujin Seo,[a] Manas Ranjan Gartia[b] and Gang Logan Liu*[bc]

Received 25th June 2014
Accepted 6th August 2014

DOI: 10.1039/c4nr03562c

www.rsc.org/nanoscale

True colorimetric sensing produces a linear spectral response of a single peak within the visible light range with various surrounding media refractive indices. We demonstrate how the circular arrangement of hemispheric silver nanoparticles achieves colorimetric properties without modifying the associated full-width-half-maximum values in a broad range of surrounding media refractive indices. We also show that the vertical out-of-plane arrangement of each circular array in nanoholes enhances the signal-to-noise ratio. High electric field confinement at the interface of the nanoparticles and the supporting substrate reveals the effect of the dielectric constant of the substrate and the morphology of the 3D nanoparticle arrays on achieving a single resonance peak in the visible range with a change in the surrounding refractive index. This study opens up the pathway to top-down fabricated nanostructure platform based plasmonic colorimetric sensing with a single resonance peak in the visible range. The studied rich set of tunable geometrical nanostructures enables broadening of the working optical range of the device.

## Introduction

Colorimetric sensing, a method of direct and intuitive environmental monitoring that detects chemical[1,2] and/or biological molecules,[3–5] has recently drawn huge interest. The technology functions due to changes in optical properties such as color variation which is visible to the human eye or spectral changes. High sensitivity in optical response is one of the key requirements for colorimetric sensing. The surface plasmon, or collective oscillation of free electrons at the interface between a noble metal and a dielectric material, has been considered as a good candidate for colorimetric sensing due to its sensitive response to local surrounding variation with a strong optical absorption and confinement of electric fields in a wide optical range, from the near ultra-violet[6] to infra-red region.[7] The surface plasmon polaritons with a thin metallic film[4] and the localized surface plasmon resonance (LSPR) with colloidal particles[8,9] showed colorimetric properties with high sensitivity. The application of the aforementioned phenomena to colorimetric sensing, however, has mostly been studied on nanoparticles synthesized by bottom-up chemistries. These nanoparticles have a single strong scattering LSPR peak in the visible range and a distinct color response based on the distance variation between each particle[10] as well as the surrounding media dielectric property changes.[11] Even though the spherical single-particle based colorimetric sensing shows a single scattering peak in the visible range that enables an instant, intuitive analysis of the color response, the detection is only available for media in a solution state and requires additional chemistries that control the distance between metallic particles.[2,8] In addition, broadening of the peak linewidth of high refractive index media is observed through many particle based sensing studies.[10,12,13] This acts as a barrier in maintaining the sensitivity and quality ($Q$) factor, since the $Q$ factor is proportional to the resonance frequency but reciprocal to the linewidth.

In order to avoid the limitation of sensing in the liquid phase and to precisely study the influence of distance, shape and size variations of metallic particles on the resonance peak, the top-down fabricated rectangular[14,15] and hexagonal[7,16,17] gold or silver nanoparticle arrays and nanostructures with holes[18] and nanorods[19] have been extensively studied. However, the application of many top-down fabricated nanostructures to the colorimetric sensing was limited due to the multiple peak emergence in the visible light range[20–22] and the resonance peak positions in the near infra-red region,[7,23,24] which hinder sensing in the visible range when there is a further red-shift of peaks by higher refractive index surrounding media.

In this paper, we propose a new design for colorimetric sensing with one-to-one correspondence of refractive index

[a]*Department of Materials Science and Engineering, University of Illinois at Urbana-Champaign, Urbana, IL 61801, USA*

[b]*Department of Electrical and Computer Engineering, University of Illinois at Urbana-Champaign, Urbana, IL 61801, USA*

[c]*Department of Bioengineering, University of Illinois at Urbana-Champaign, Urbana, IL 61801, USA. E-mail: loganliu@illinois.edu*

† Electronic supplementary information (ESI) available. See DOI: 10.1039/c4nr03562c

change to spectral shift: a tunable plasmonic circular array of nanoparticles on a solid template fabricated by a top-down process. This achieves a free-standing sensing platform with linearity among the plasmonic resonance peak shift and the refractive index variation of the surrounding media. We report that this circular arrangement of nanoparticles can bring a single distinct resonance peak in the visible wavelength and its peak position can be easily tuned by varying the substrate refractive index and the morphology of the particle arrays.

We also demonstrate a simple and easy way to achieve a higher signal-to-noise ratio (SNR), defined as the ratio between the peak power and the background noise power, by introducing additional circular arrays arranged in the vertical direction. The power was calculated by integrating the spectra in the wavelength range of signals, and the background noise power was evaluated with a model without nanoparticles in the nanohole. Achieving a high SNR has been of interest for surface plasmon based sensing, since it helps to improve the detection limit and accurately measure the plasmonic peak shift upon a change in the refractive index. Zynio *et al.*[25] proposed to use bimetallic layers for improving the SNR and Dahlin *et al.*[26] and Wang *et al.*[27] suggested improving the measuring equipment and method; however, these are not direct breakthroughs for enhancing the SNR of a surface plasmon based sensor. We confirmed that out-of-plane coupling achieved solely with the addition of more layers produces a better SNR with a linearly increasing signal intensity corresponding to the number of layers and the enhancement of the smoothness of peaks and the *Q* factor as well. This occurs due to full width at half maximum (FWHM) reduction.

In the previous study, we used a promising top-down fabrication method to form hemispherical nanoparticles in a circular array with properties similar to those of spherical particles produced by a bottom-up approach (see ESI†).[28] Even though the nanoparticles formed by the top-down fabrication has an asymmetric, hemispherical shape which results in two asymmetric surface plasmon resonance frequencies (ESI Fig. S1a†), the optical properties can be tuned similarly to that of a single perfect sphere with a single peak in the visible range by arranging the particles in a circle. We demonstrate the possible nanoparticle arrangements by numerical calculation, which show a very sensitive colorimetric response of a single prominent resonance peak with a narrow bandwidth in comparison with conventional rectangular nanoparticle arrays.

## Results and discussion

### Tunable plasmonic resonance

The scanning electron microscopy (SEM) images in ESI Fig. S2a and b† show that hemispheric silver nanoparticles are attached on the sidewall of the cup region and that most particles are arranged in a circle. On average, eight hemispheric nanoparticles with a diameter of 30 nm were attached on the sidewall and this arrangement was simulated in the three-dimensional finite-difference time-domain (FDTD) software, utilizing the FDTD program from Lumerical Solutions, Inc. Fig. 1a and b

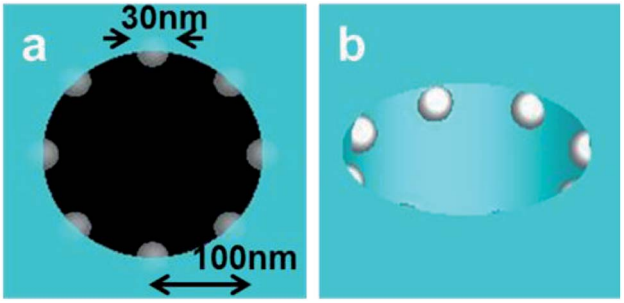


Fig. 1 Schematic representation of the simulated sidewall nanoparticles on the periodic nanoholes in the (a) *x*,*y*-plane view and (b) tilted perspective view.

demonstrate the arrangement of eight nanoparticles in a circular array using FDTD simulation. A circular array of eight hemispheres and a silver toroid structure on the flat polymer substrate with a refractive index of 1.56 were also calculated for the effect of the discrete particle array in a circular arrangement on determining the plasmon resonance, differentiating from that of the silver toroid structure which can be considered as an infinite number of hemispheres in a circular array. The silver dielectric properties were taken from Palik[29] and the uniform 0.8 nm mesh was used on the structure. Periodic boundary conditions with a periodicity of 320 nm in the *x*- and *y*-directions were imposed.

We first demonstrate how the circular array responds to the variation of the inter-particle distance, compared to conventional square array and toroid structure responses. The distance between each hemispheric particle in the circular array was controlled by varying the diameter of the whole array, from 120 nm to 200 nm. An equivalent inter-particle distance was applied to the square periodic array of hemispheric nanoparticles. Fig. 2 shows the effect of increasing inter-particle distance and all four models consistently showed a red-shift of the peak wavelength with decreasing inter-particle distance. The red-shift of peaks with closer particles agrees well with the previous dimer LSPR studies.[30,31] The red-shift of the resonance wavelength of the particles is due to the reduced net dipole power between nanoparticles, which results from the attraction between induced opposite charges accumulating on each end of the particles along the light polarization axis.[32] The toroid structure from Fig. 2c also showed a blue shift of the peak wavelength corresponding to an increase in the toroid diameter. However, the shift of the peak wavelength (2.5 nm) is minimal compared to the discrete particle cases (Fig. 2a (12.5 nm), Fig. 2b (22.5 nm) and Fig. 2d (17.5 nm)). Since the toroid structure can be considered as a continuous arrangement of infinite hemispheric particles, there is no localized surface plasmon excited on a discrete nanoparticle and hence, there is limited influence of variation in the toroid's diameter. The effect of inter-particle distance does not yet reveal whether or not the circular array of the nanoparticle model is good for colorimetric sensing, but this clearly demonstrates that the resonance peak wavelength can be tuned by geometrical control of the nanoparticle circular array structure.

 

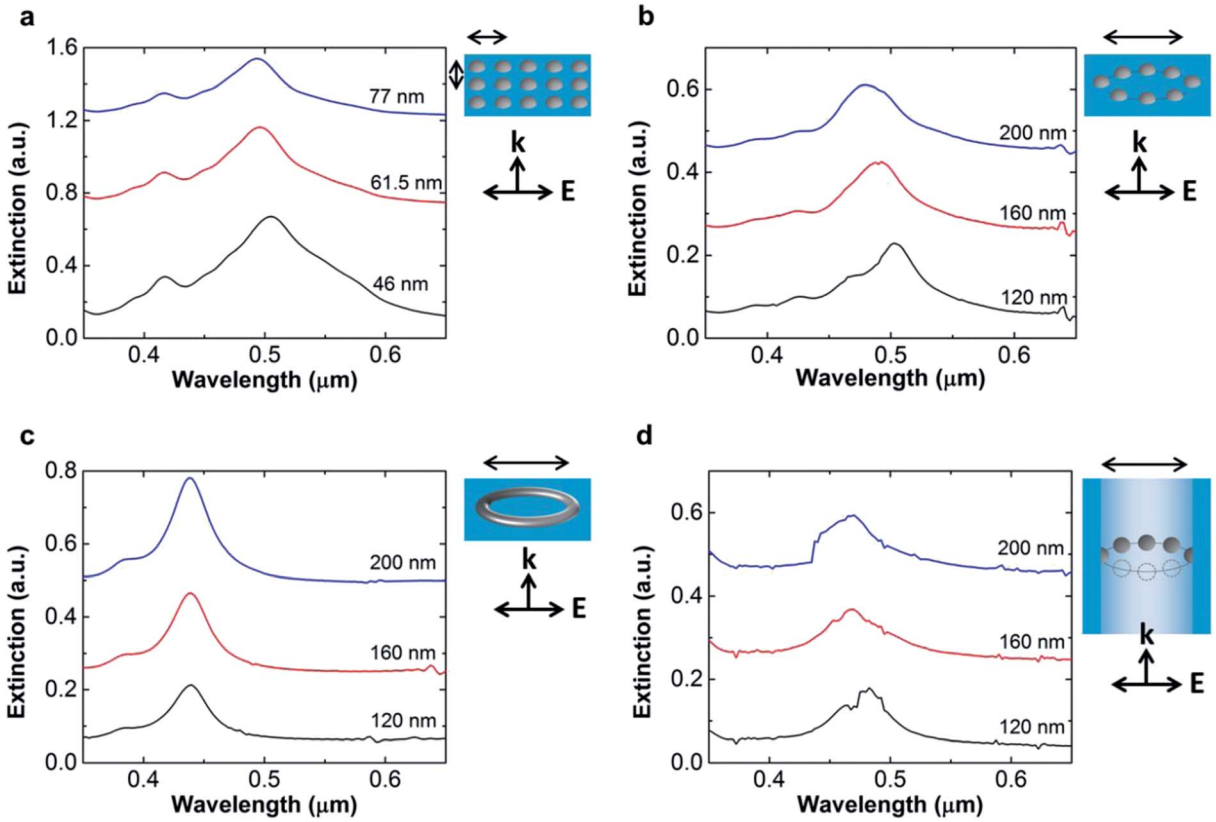


Fig. 2 Extinction spectra with varying inter-particle distances and toroid's diameters. Extinction spectra of (a) the rectangular array of nanoparticles spaced equally as the distance between each adjacent nanoparticle in the circular array with a diameter of 120 nm, 160 nm, and 200 nm, (b) the circular array of nanoparticles on a flat substrate, (c) the toroid metallic ring structure on a flat substrate, and (d) the circular array of nanoparticles attached on the vertical sidewall inside a hole were compared with an increasing diameter of the array.

### FWHM and *Q*-factor

The linewidth of the resonance was measured for the square array of nanoparticles and the circular array of nanoparticles on each flat surface and within the nanoholes. Compared to the square array, the circular arrays of nanoparticles on the flat surface and inside of the holes had a relatively smaller FWHM. The square array has a FWHM of 82.5 nm, whereas the circular arrays on the flat substrate and inside the holes have a FWHM of 65 nm and 52.5 nm respectively. This indicates that the circular arrays have better sensitivity with a higher *Q* factor as an optical sensor.

The lateral in-plane coupling of the LSPR was studied by varying the number of particles in each circular array in Fig. 3a. Having four and eight nanoparticles on the sidewall both result in a peak position of 470 nm, whereas a circular array with 16 nanoparticles has a red-shifted peak wavelength at 500 nm. This indicates lowering of the overall energy. The linewidth broadening in the 16 particles case can be attributed to extra losses in the metal due to increased surface scattering. The calculated surface charge distributions associated with the 16 particles in Fig. 3b show large effective dipole moments that align and oscillate in phase. This leads to higher resonant coupling efficiency and high radiative losses (scattering), thus increasing the linewidth of radiation. On the other hand, the higher-energy

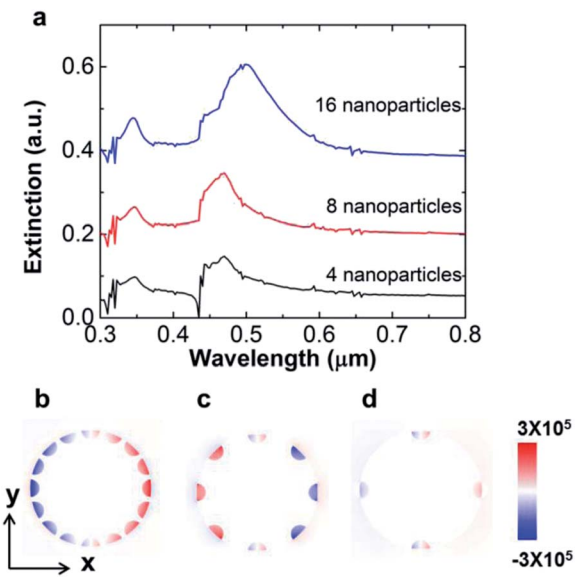


Fig. 3 (a) Extinction spectra from a circular array with 16 nanoparticles, 8 nanoparticles, and 4 nanoparticles. The current density distribution, *J*, of (b) 16, (c) 8, and (d) 4 nanoparticles on the vertical sidewall at each peak wavelength is presented.

dipolar modes for four and eight particles case in Fig. 3c and d show surface charges that are partially canceled due to phase-retardation effects resulting in lower effective dipole moments. The reduced dipole moment leads to relatively lower resonant coupling efficiency and reduced radiative scattering. Hence, the four and eight nanoparticle cases have smaller linewidths compared to the 16 nanoparticles case. In terms of sensor application, having eight hemispheric nanoparticles in an array is preferable due to its smaller FWHM than the 16 hemispheric nanoparticle circular array. When we compare the spectrum of the four nanoparticle array with that of the eight nanoparticle array, the SNR of the four nanoparticle case is lower than the latter due to a smaller extinction peak intensity, which is 0.075 compared to the 0.114 extinction value of the eight nanoparticle case. Thus, we decided to further study the eight nanoparticle circular array for better sensing applications.

### Multiple layer stacking

Achieving a high SNR of the extinction spectrum is crucial to an actual sensor application. We report that the peak intensity of the circular array is enhanced by vertically stacking the circular array layers as shown in Fig. 4. In Fig. 4a, the extinction peak wavelength red-shifts from 470 nm with a single layer to 480 nm with triple and quintuple layers of the nanoparticle array. The triple and quintuple layers have a fixed vertical distance of 100 nm between the centers of each nanoparticle array layer. The vertical inter-layer distance effect on the extinction spectra will be explained in Fig. 4b. In addition, the SNR linearly increases by 4.15-fold for the quintuple layer compared to the single layer, while the FWHM increases only by 1.2-fold. The increase in intensity by stacking the multiple layers is due to the induced magnetic field between each layer of nanoparticles. This creates an electric current orthogonal to the magnetic field, resulting in an increase in intensity. Thus, introducing more scattering objects such as silver nanoparticles in the direction of light propagation instead of in the light polarization direction is the key to increasing the signal intensity while retaining most of the optical properties of the original single layer.

Fig. 4b shows the effect of the inter-layer distance for the triple layer case. When the vertical inter-layer particle edge-to-edge distance decreases from 220 nm to 5 nm, the resonance peak at 480 nm blue-shifts to 475 nm. Similarly, the FWHM is decreased by 5 nm or ~10%. Thus, the overall $Q$ factor improves with increased resonance frequency and narrower linewidth of the peak as the inter-layer distance decreases. It was reported that the $Q$ factor of plasmonic resonators is independent of the geometry and dielectric environment of the nanostructure.[33] In contrast, here we show that the $Q$-factor can be affected by

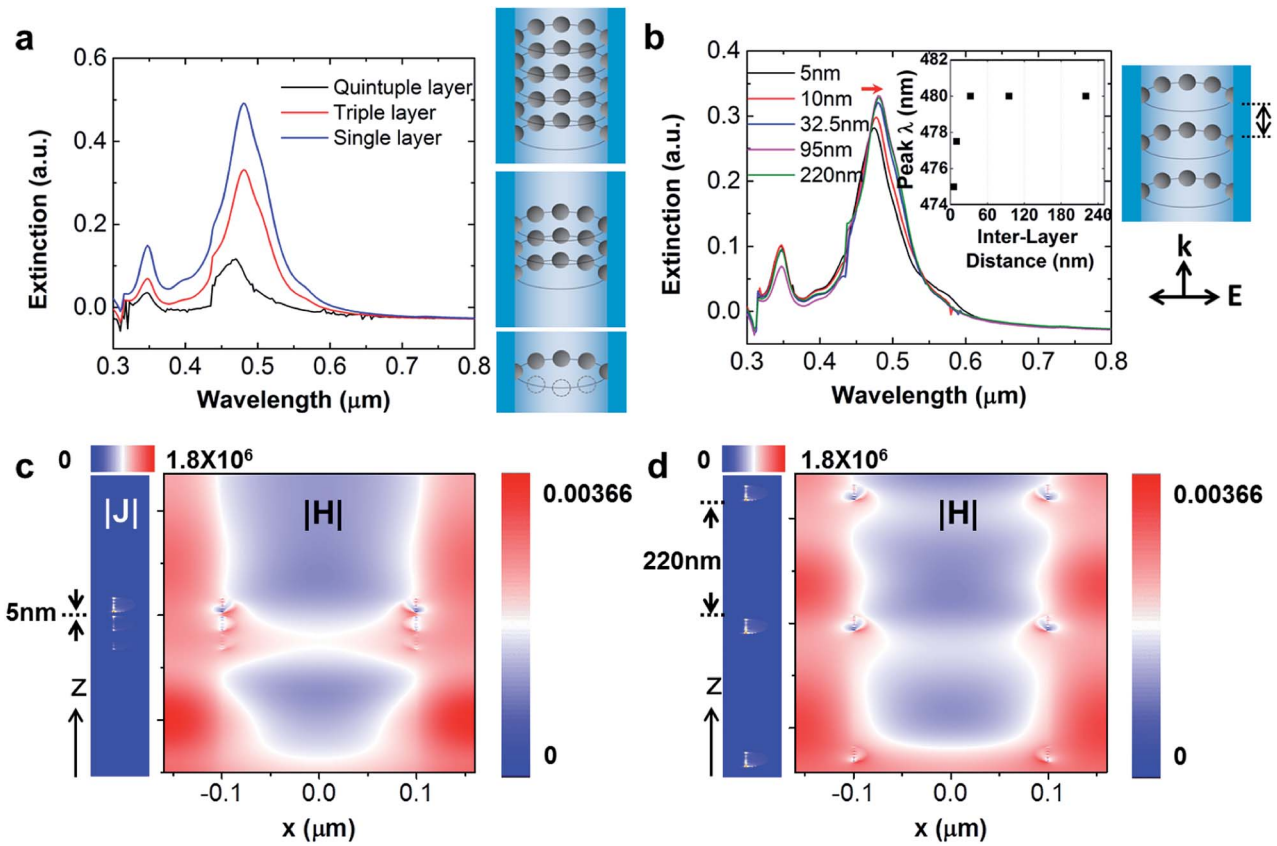


Fig. 4 (a) Extinction spectra with different numbers of layers and (b) with varying distances between each layer. (c and d) The current density (|$J$|) and the magnetic field (|$H$|) of the triple circular array stacks with (c) 5 nm and (d) 220 nm edge-to-edge inter-layer distance. All circular arrays have a fixed hole diameter of 200 nm.

 

vertically stacking the arrays of the nanostructure. The observed blue-shift of the peak wavelength with vertical coupling is similar to the response of the LSPR peak shift with the excitation light polarized orthogonal to the inter-particle axis of linearly arranged two or more nanoparticles.[32,34] When the incident light is polarized perpendicular to the inter-particle axis, it leads to the accumulation of charges with identical polarity on the opposite sides of the gap. Identical charges repel each other and hence increased restoring forces result in decreased $\lambda_{LSPR}$. On the other hand, the blue-shift of the resonance wavelength by 5 nm from a decreased inter-layer gap distance is smaller than that from the in-plane orthogonal coupling between two nanoparticles, which is a few tens of nm.[32] The main reason why the resultant response from the nanoparticle circular array in nanoholes is smaller than the conventional LSPR peak shift driven from two circular nanoparticles with s-polarized light is the non-spherical shape of the nanoparticles on the sidewall. The electric field developed on the hemispheric nanoparticle is weaker due to the asymmetry, compared to the perfect spherical nanoparticles. In addition, different interfacial dielectric properties on each nanoparticle in the direction of light polarization, which are air inside the hole and the substrate, contribute to non-uniform distribution of the electric field and charges at each end of the nanoparticles. Therefore, there is less coupling force among electric dipoles, resulting in a smaller blue-shift. The circular array in the nanoholes, however, did not exhibit broadening of peak or loss in the peak intensity. This indicates that the vertical coupling of the collective resonance mode of the particle array effectively confines the field without the loss of $Q$ factor.

We further examined the vertical coupling of the collective plasmonic mode of each layer by presenting the current density, $|J|$, and the magnetic field distribution, $|H|$, of the two cases, with and without vertical coupling, at each resonance peak wavelength in Fig. 4c and d. Fig. 4c clearly shows the vertical coupling of the fields which is absent in Fig. 4d. The current density and the magnetic field with vertical coupling are no longer uniform across three circular array layers but concentrated on the top-most layer. The magnetic field is also highly confined in-plane inside the cylindrical hole, which verifies a higher $Q$-factor with a smaller layer-to-layer separation gap. The charge distribution map (see ESI Fig. S3†) shows individual dipole formation on each nanoparticle with a larger displacement between layers, but single dipole formation among the three array stack with a shorter displacement. As a larger net

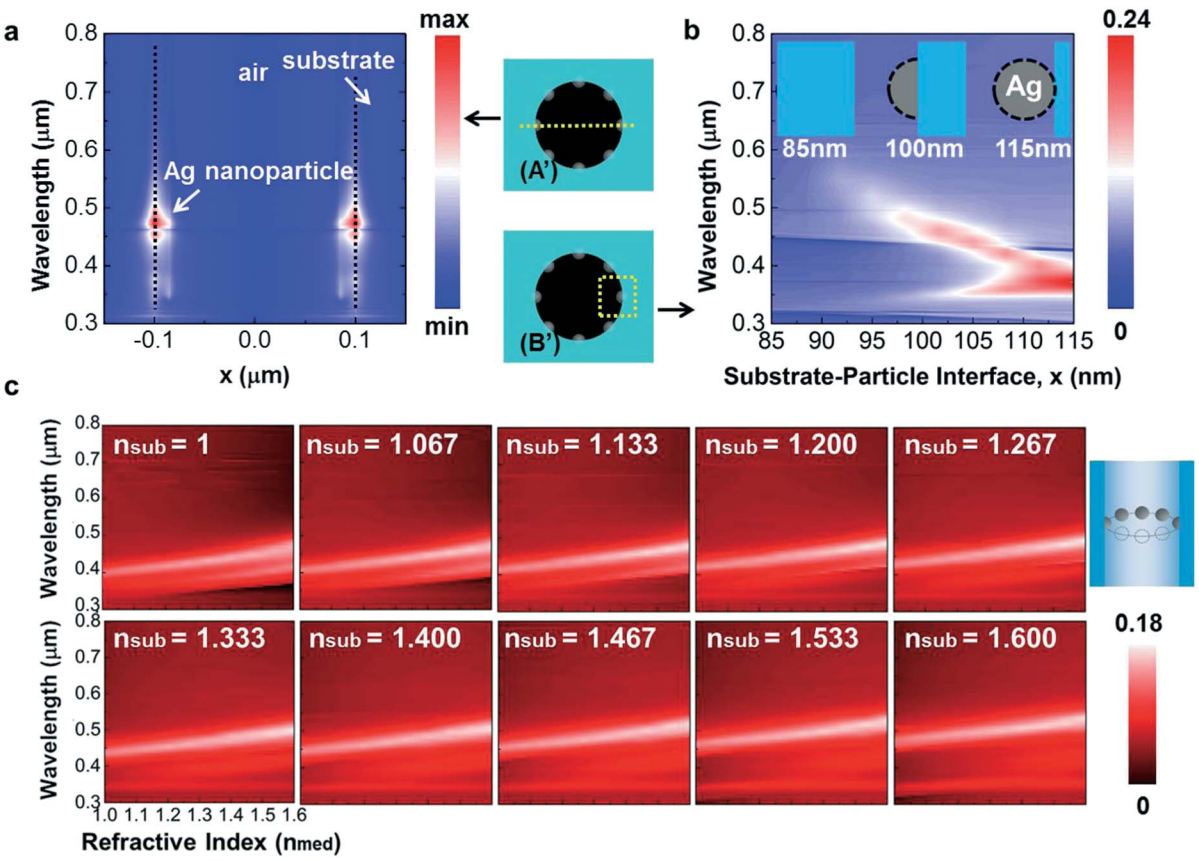


Fig. 5 The effect of the dielectric properties of the substrate and the morphology of the particle on achieving a single resonance peak in the visible light range. (a) The electric field ($|E_z|$) distribution showing the field confinement at the interface between the particle and the substrate at the line crossing two nanoparticles in $x$-directions. (b) The effect of the morphology of the nanoparticle on the extinction spectra by varying the substrate interface position while fixing the particle center position. (c) The extinction spectral response of a single circular array of eight nanoparticles to the variation of the substrate and the surrounding media refractive indices, ranging from 1 to 1.6 respectively.

electric dipole is built among the layers with a shorter interlayer distance, a larger magnetic field loop across the layers is produced. A similar magnetic field enhancement was observed with nanorod pairs with opposite current directions.[35,36]

### Morphology of nanoparticles

The electric field on the nanoparticle circular array is mainly confined at the interface between the dielectric cylindrical hole substrate and the silver particle. Fig. 5a shows a high electric field ($E_z$) located in the contact region of the metallic nanoparticle with the cylindrical wall. A single circular array with eight hemispheric nanoparticles attached inside the 200 nm cylindrical hole was chosen for this numerical analysis. Since the electric field is mostly confined at the interface between the silver particle and the substrate sidewall, the plasmonic peak wavelength should respond according to the change of the dielectric properties of the substrate, which is in contact with the silver nanoparticles. The magnitude of the electric field is also dependent on the morphology of the nanoparticles, which in turn defines the contact area.

Fig. 5b shows the effect of changing the interfacial area between the nanoparticle and the substrate sidewall by gradually increasing the substrate hole diameter from 85 nm, no nanoparticles exposed and existed, to 115 nm, a complete exposure of silver spherical particles attached on the sidewall. The size of the particles was consistent which were 30 nm in diameter and the center of each nanoparticle was fixed in a circular arrangement inside the cylindrical hole structure with a refractive index of 1.56. When the hemispheric particle is exposed to air, a distinguishing extinction peak emerges. The peak wavelength blue-shifts, as a larger portion of the particles is exposed outside of the sidewall, forming a less interfacial area. The circular arrangement of perfect spherical nanoparticles has the peak position similar to the Mie scattering peak wavelength (see ESI Fig. S1a†).

### Sensitivity to environmental changes

The supporting substrate dielectric properties bring an additional degree of freedom in tuning the plasmonic resonance peak position. The gradual increase of the surrounding refractive index of the dielectric material usually leads to the red-shift of the resonance peak wavelength as shown in single nanoparticle studies.[37,38] However, the relationship between the plasmonic properties and the refractive index of the supporting substrate is scarcely studied. Fig. 5c shows the map of extinction spectra from the eight hemispherical nanoparticle circular array by varying the surrounding media refractive indices from $n_{med} = 1$ to 1.6 (noted on the $x$-axis) as well as varying the substrate refractive indices from $n_{sub} = 1$ to 1.6. The resonance peak changes from 400 nm to 480 nm when ($n_{sub}$, $n_{med}$) changes from (1, 1) to (1.6, 1). It should be noted that the circular array of hemispheres does not always exhibit a single resonance peak in

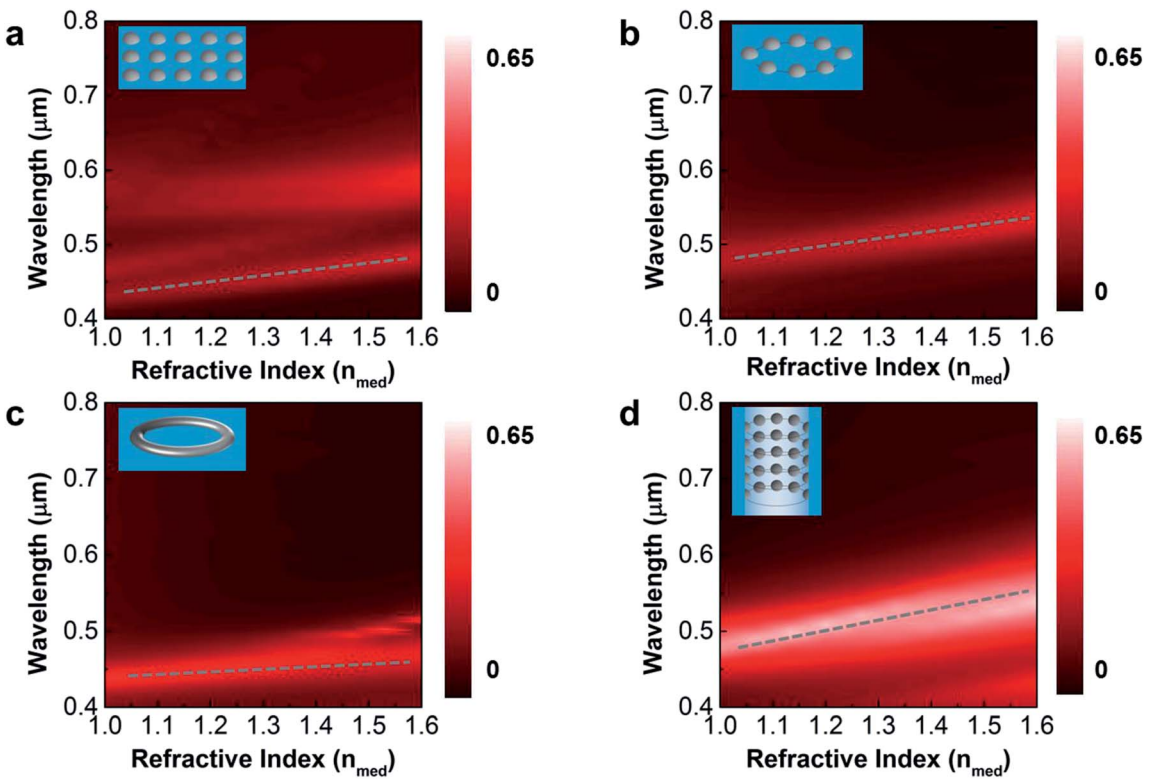


Fig. 6 Extinction spectra of four models with the change in refractive index of surrounding media: (a) the square array of hemispheric nanoparticles on a flat surface, (b) the circular array on a flat surface, (c) the toroid structure on a flat surface, and (d) the quintuple layer stack of the eight nanoparticle circular array on a vertical sidewall of nanoholes. The greatest sensitivity and highest SNR were observed with the quintuple array stack.

 

the visible range. For example, when the $(n_{sub}, n_{med}) = (1, 1)$, the extinction spectrum becomes similar to the hemisphere's scattering spectrum (ESI Fig. S1a†) with double peaks due to its asymmetric structure, inducing a multipolar resonance mode.[39] However, as the substrate refractive index increases ($n_{sub} > 1.4$), the main peak starting from 400 nm red-shifts and it becomes prominent compared to the second peak in the lower wavelength range. Therefore, the substrate dielectric properties such as the refractive index are some of the key parameters to control the starting resonance peak position and to achieve colorimetric sensing modality.

To utilize the actual model in the real colorimetric sensor application, a linear response of the scattering peak spectra with the media dielectric property change is desired for the direct intuitive calibration and interpretation of the data. The colorimetric responses of the four models listed below to varying surrounding media are depicted in Fig. 6: (1) the stacked nanoparticle circular array on the cylindrical hole sidewall, (2) the circular array on the flat surface, (3) a half toroid structure on the flat surface, and (4) the conventional square array of hemispheric nanoparticles. The square array (Fig. 6a), which had a broad peak compared to the circular array and the toroid structure in Fig. 2c, eventually exhibited double peaks with a high surrounding refractive index. This result agrees well with the experimental result from Y. Lin *et al.*[40] for the square nanodot array. Unlike the square array, the toroid structure and the circular array whether on a flat surface or inside the cylindrical hole had a single distinct peak in the visible range even in the high refractive index surrounding medium. The sensitivity, which is the peak shift per refractive index unit (RIU), was the greatest for the quintuple circular array with the cylindrical hole structure (128.6 nm per RIU), compared to the square array (106.3 nm per RIU), the circular array on a flat substrate (87.5 nm per RIU) and the toroid structure (65.2 nm per RIU).

Among the four models in Fig. 6, the quintuple stack of eight nanoparticle circular arrays on the vertical sidewall (Fig. 6d) had the highest SNR. The SNR can be further improved by adding more layers on top as depicted in Fig. 4a. In addition, the sensitivity is also the highest for the stacked circular array. A single circular array on the flat substrate (Fig. 6b) has comparable sensitivity, but its low intensity makes it less attractive for the sensor application.

Achieving a high *Q*-factor is another necessary factor in colorimetric sensing. The conventional colloidal colorimetric sensing with single particle induced LSPR has peak broadening in high refractive index media (see ESI Fig. S1b† with single particle Mie scattering numerical analysis results). In air, the single particle based sensing seems to be a better detector with a high *Q*-factor, but its FWHM was increased by 57.8% after changing the surrounding refractive index from 1 to 1.6. The circular array, however, had a 34.7% increase in the FWHM with the same refractive index variation. This indicates that the circular array has better colorimetric properties with better consistency in the *Q*-factor compared to the conventional single particle (Mie scattering) based colorimetric sensor.

# Conclusions

The nanoparticle circular array represents one of the strong designs for colorimetric sensing with a less noise level. This eliminates the need for a solvent, contrary to the conventional colloidal nanoparticle colorimetric sensing. It provides a solid template for detecting environmental changes. Out-of-plane coupling produced by stacking the circular arrays enables to achieve extinction spectra with stronger peak intensities as well as a 4.15-fold increase in the SNR with a quintuple layer. A higher SNR can be achieved by stacking more layers. In addition, careful selection of substrate materials as well as precise substrate and nanoparticle geometrical modeling is crucial for achieving the single resonance peak in the visible range. The parameters controlling the resonance peak position are the distance between each particle, the refractive indices of the surrounding medium and the substrate, and the morphology of the nanoparticle. Stronger in-plane LSPR coupling, which involves a smaller cylindrical hole diameter and a larger number of particles in one layer, leads to the red-shift of the resonance peak wavelength. Out-of-plane coupling, on the other hand, results in the blue-shift of the resonance peak wavelength and decrease in the FWHM by 5 nm for the triple layer case. The *Q* factor, therefore, was improved by inducing a stronger out-of-coupling with a shorter inter-layer distance. We additionally report that stacked circular arrays of nanoparticles have advantage in retaining the *Q* factor with less broadening of the resonance peak, compared to the Mie scattering based colloidal nanoparticle plasmonic sensing platform. By optimizing the colorimetric properties by tuning the geometrical and optical parameters studied, the nanoparticle circular array as a colorimetric sensor offers a broad range of color selection or spectrally active regions for interesting potential applications.

# Acknowledgements

This work is partially supported by the U.S. Department of Energy under Grants DE-FG02-07ER46453 and DE-FG02-07ER46471.

# Notes and references

1 S. H. Lim, L. Feng, J. W. Kemling, C. J. Musto and K. S. Suslick, *Nat. Chem.*, 2009, **1**, 562–567.
2 W. Zhao, M. A. Brook and Y. Li, *ChemBioChem*, 2008, **9**, 2363–2371.
3 R. Elghanian, J. Storhoff, R. C. Mucic, R. L. Letsinger and C. A. Mirkin, *Science*, 1997, **277**, 1078–1081.
4 C. L. Wong, G. C. K. Chen, X. Li, B. K. Ng, P. Shum, P. Chen, Z. Lin, C. Lin and M. Olivo, *Biosens. Bioelectron.*, 2013, **47**, 545–552.
5 H. Li and L. Rothberg, *J. Am. Chem. Soc.*, 2004, **126**, 10958–10961.
6 M.-W. Chu, P. Sharma, C.-P. Chang, S. C. Liou, K.-T. Tsai, J.-K. Wang, Y.-L. Wang and C. H. Chen, *Nanotechnology*, 2009, **20**, 235705.

7 A. I. Kuznetsov, A. B. Evlyukhin, M. R. Gonçalves, C. Reinhardt, A. Koroleva, M. L. Arnedillo, R. Kiyan, O. Marti and B. N. Chichkov, *ACS Nano*, 2011, **5**, 4843–4849.
8 J. Storhoff and R. Elghanian, *J. Am. Chem. Soc.*, 1998, **120**, 1959–1964.
9 N. Nath and A. Chilkoti, *Anal. Chem.*, 2002, **74**, 504–509.
10 S. Chah, M. R. Hammond and R. N. Zare, *Chem. Biol.*, 2005, **12**, 323–328.
11 A. D. McFarland and R. P. Van Duyne, *Nano Lett.*, 2003, **3**, 1057–1062.
12 K. Aslan, J. R. Lakowicz and C. D. Geddes, *Anal. Biochem.*, 2004, **330**, 145–155.
13 F. Xia, X. Zuo, R. Yang, Y. Xiao, D. Kang, A. Vallée-Bélisle, X. Gong, J. D. Yuen, B. B. Y. Hsu, A. J. Heeger and K. W. Plaxco, *Proc. Natl. Acad. Sci. U. S. A.*, 2010, **107**, 10837–10841.
14 A. Hohenau, J. Krenn, J. Beermann, S. Bozhevolnyi, S. Rodrigo, L. Martin-Moreno and F. Garcia-Vidal, *Phys. Rev. B: Condens. Matter Mater. Phys.*, 2006, **73**, 155404.
15 C. L. Haynes, A. D. McFarland, L. Zhao, R. P. Van Duyne and G. C. Schatz, *J. Phys. Chem. B*, 2003, **107**, 7337–7342.
16 H. Portalès, N. Pinna and M.-P. Pileni, *J. Phys. Chem. A*, 2009, **113**, 4094–4099.
17 S. Kim, N. Cheng, J.-R. Jeong, S.-G. Jang, S.-M. Yang and W. T. S. Huck, *Chem. Commun.*, 2008, 3666–3668.
18 S.-H. Chang, S. K. Gray and G. C. Schatz, *Opt. Express*, 2005, **13**, 3150–3165.
19 A. Ono, J. Kato and S. Kawata, *Phys. Rev. Lett.*, 2005, **95**, 267407.
20 D. P. Lyvers, J.-M. Moon, A. V Kildishev, V. M. Shalaev and A. Wei, *ACS Nano*, 2008, **2**, 2569–2576.
21 M. Bora, B. J. Fasenfest, E. M. Behymer, A. S.-P. Chang, H. T. Nguyen, J. A. Britten, C. C. Larson, J. W. Chan, R. R. Miles and T. C. Bond, *Nano Lett.*, 2010, **10**, 2832–2837.
22 A. Krishnan, T. Thio, T. J. Kim, H. J. Lezec, T. W. Ebbesen, P. A. Wolff, J. Pendry, L. Martin-Moreno and F. J. Garcia-Vidal, *Opt. Commun.*, 2001, **200**, 1–7.
23 O. Vazquez-Mena, T. Sannomiya, L. G. Villanueva, J. Voros and J. Brugger, *ACS Nano*, 2011, **5**, 844–853.
24 Y. Shen, J. Zhou, T. Liu, Y. Tao, R. Jiang, M. Liu, G. Xiao, J. Zhu, Z.-K. Zhou, X. Wang, C. Jin and J. Wang, *Nat. Commun.*, 2013, **4**, 2381.
25 S. A. Zynio, A. V. Samoylov, E. R. Surovtseva, V. M. Mirsky and Y. M. Shirshov, *Sensors*, 2002, **2**, 62–70.
26 A. B. Dahlin, J. O. Tegenfeldt and F. Höök, *Anal. Chem.*, 2006, **78**, 4416–4423.
27 X. Wang, M. Jefferson, P. C. D. Hobbs, W. P. Risk, B. E. Feller, R. D. Miller and A. Knoesen, *Opt. Express*, 2011, **19**, 107–117.
28 M. R. Gartia, A. Hsiao, A. Pokhriyal, S. Seo, G. Kulsharova, B. T. Cunningham, T. C. Bond and G. L. Liu, *Adv. Opt. Mater.*, 2013, **1**, 68–76.
29 *Handbook of Optical Constants of Solids*, ed. E. D. Palik, Academic Press, New York, 1985.
30 C. Sönnichsen, B. M. Reinhard, J. Liphardt and A. P. Alivisatos, *Nat. Biotechnol.*, 2005, **23**, 741–745.
31 Z. B. Wang, B. S. Luk'yanchuk, W. Guo, S. P. Edwardson, D. J. Whitehead, L. Li, Z. Liu and K. G. Watkins, *J. Chem. Phys.*, 2008, **128**, 094705.
32 W. Rechberger, A. Hohenau, A. Leitner, J. R. Krenn, B. Lamprecht and F. R. Aussenegg, *Opt. Commun.*, 2003, **220**, 137–141.
33 F. Wang and Y. R. Shen, *Phys. Rev. Lett.*, 2006, **97**, 206806.
34 S. Yin, Q. Deng, X. Luo, C. Du and Y. Zhang, *J. Appl. Phys.*, 2008, **104**, 024308.
35 R. Ameling and H. Giessen, *Laser Photonics Rev.*, 2013, **7**, 141–169.
36 A. Christ, O. J. F. Martin, Y. Ekinci, N. a. Gippius and S. G. Tikhodeev, *Nano Lett.*, 2008, **8**, 2171–2175.
37 G. J. Nusz, S. M. Marinakos, A. C. Curry, A. Dahlin, F. Höök, A. Wax and A. Chilkoti, *Anal. Chem.*, 2008, **80**, 984–989.
38 B. Lahiri, A. Z. Khokhar, R. M. De La Rue, S. G. McMeekin and N. P. Johnson, *Opt. Express*, 2009, **17**, 1107–1115.
39 E.-A. You, W. Zhou, J. Y. Suh, M. D. Huntington and T. W. Odom, *ACS Nano*, 2012, **6**, 1786–1794.
40 Y. Lin, Y. Zou, Y. Mo, J. Guo and R. G. Lindquist, *Sensors*, 2010, **10**, 9397–9406.